Resonant metamaterial absorbers for infrared spectral filtering: quasimodal analysis, design, fabrication, and characterization

Benjamin Vial,[1,2,*] Guillaume Demésy,[1] Frédéric Zolla,[1] André Nicolet,[1] Mireille Commandré,[1] Christophe Hecquet,[1] Thomas Begou,[1] Stéphane Tisserand,[2] Sophie Gautier,[2] and Vincent Sauget[2]

[1]*Centrale Marseille, Aix Marseille Université, CNRS, Institut Fresnel, UMR 7249, 13013 Marseille, France*
[2]*Silios Technologies, ZI Peynier-Rousset, rue Gaston Imbert Prolongée, 13790 Peynier, France*
**Corresponding author: benjamin.vial@fresnel.fr*

Received February 21, 2014; revised April 22, 2014; accepted April 22, 2014;
posted April 25, 2014 (Doc. ID 206107); published May 22, 2014

We present a modal analysis of metal–insulator–metal (MIM)-based metamaterials in the far infrared region. These structures can be used as resonant reflection bandcut spectral filters that are independent of the polarization and direction of incidence. We show that this resonant reflection dip is due to the excitation of quasimodes (modes associated with a complex frequency) leading to quasi-total absorption. We have fabricated large area samples made of chromium nanorod gratings on top of Si/Cr layers deposited on silicon substrate. Measurements by Fourier transform spectrophotometry show good agreement with finite element simulations. A quasimodal expansion method is applied to obtain a minimal resonant model that fits well full wave simulations and that highlights excitation conditions of the modes.

OCIS codes: (000.4430) Numerical approximation and analysis; (050.0050) Diffraction and gratings; (050.5745) Resonance domain; (160.3918) Metamaterials; (220.4241) Nanostructure fabrication.
http://dx.doi.org/10.1364/JOSAB.31.001339

1. INTRODUCTION

Structuration of metallic surfaces with typical sizes smaller than the wavelength can lead to spectacular resonant effects. More than one century ago, anomalies in reflection of metallic gratings were discovered by Wood [1], and substantial pioneering work [2,3] has highlighted the role of surface plasmons polaritons in the anomalous reflection in mono- and bi-periodic gratings. These resonances can be used to fashion various reflection and transmission spectra. In particular, total absorption phenomena in different metamaterial type [4–8] from the microwave to optical regime have recently attracted a lot of interest because of their potential application in sensing [9], tunable frequency selective microbolometers [10,11], or solar cells [4]. One family of metamaterial has been extensively studied that is based on a metal–insulator–metal (MIM) configuration [8,12–15], because it can lead to polarization and angle independent resonant perfect absorption. This is the kind of structure we study both numerically and experimentally in this article with the aim of using it as bandcut reflection filters in the infrared that can be tuned by adjusting the periodicity of the grating.

Besides the calculation of diffraction efficiencies and absorption spectra, our approach to study the resonant phenomena in such metamaterials is to compute the eigenmodes and eigenfrequencies of such open electromagnetic systems. The study of poles and zeros of the scattering operator [16,17] and of their associated leaky modes leads to significant insights into the properties of metamaterials [18–21] and eases the conception of diverse optical devices [22–26] because it provides a simple picture of the resonant processes at stake. From the resolution of a spectral problem, one obtains complex eigenfrequencies. When considering a single isolated resonance, the real part is the resonant frequency and the imaginary part is related to its bandwidth. Actually, the resonance can be non-Lorentzian so that the definition of the bandwidth may be problematic. Anyway, the variations in scattering spectra with frequency are all the more curt when the imaginary part of the eigenvalue is weak. This simplified picture is not valid anymore when several resonances overlap, leading to more complex diffracted spectra. Resonant scattering is expected when shining light with frequency around the resonant frequency. We report here a numerical spectral analysis of MIM arrays that allows us to optimize parameters for infrared reflection bandcut filters. The spectral position of the reflection dip can be adjusted by varying the periodicity of the grating. Large area samples with different periods have been fabricated and characterized by FTIR spectroscopy, and experimental data agree well with the numerical predictions of both calculated reflection spectra and complex eigenvalues. Specifically, the high angular tolerance of the filters is demonstrated experimentally and numerically.

The eigenvectors and eigenvalues are intrinsic properties of the studied system that depend on the opto-geometrical parameters but are in essence independent of the excitation conditions. Recently, quasimodal expansion techniques have been developed to provide a clear physical picture of resonant scattering processes in 2D [27,28] and 3D [29,30] photonic systems. In this article we provide a systematic method to characterize the excitation of a given mode. By expanding the scattered field onto the eigenmode set, we can compute

the coupling coefficient that characterizes the strength of the interaction of incident light with a mode. This method is illustrated in the case of a MIM array, showing the resonant nature of the reflection dip and providing a reduced-order model with two degenerate leaky modes that fits well full wave finite elements calculation.

2. SETUP OF THE PROBLEM AND THEORETICAL BACKGROUND

A. Diffraction Problem

The geometry of the structures studied in this article is represented in Fig. 1(a) and consists of three layers. The top layer is made of a square array with period d along both Ox and Oy of cylindrical chromium nanorods with diameter D and thickness h_r. The bottom layer is a continuous chromium film of thickness h_m. These two metallic layers are separated by an amorphous silicon film of thickness denoted h_i. The incident medium (superstrate) is air with permittivity $\varepsilon^+ = 1$, and the structure is deposited on a silicon substrate with permittivity ε^-. The permittivity of chromium is described by a Drude–Lorentz model [31] $\varepsilon_\mathrm{Cr}(\omega) = 1 - \omega_\mathrm{p}^2/(\omega^2 + i\omega\Gamma)$, with $\omega_\mathrm{p} = 6.903 \cdot 10^{15}$ rad $\cdot$ s^{-1} and $\Gamma = 8.288 \cdot 10^{13}$ rad $\cdot$ s^{-1}. The refractive index of bulk (for the substrate) and amorphous silicon (for the Si layer) are taken from tabulated data [32]. All materials are assumed to be nonmagnetic ($\mu_r = 1$).

We consider here the time-harmonic regime with $\mathrm{e}^{-i\omega t}$ dependence. The structure is illuminated by a plane wave $\boldsymbol{E}^\mathrm{inc} = \boldsymbol{A}_0^\mathrm{e} \exp(i\boldsymbol{k}^+ \cdot \boldsymbol{r})$ with

$$\boldsymbol{k}^+ = \begin{vmatrix} \alpha \\ \beta \\ \gamma \end{vmatrix} = k^+ \begin{vmatrix} -\sin\theta_0 \cos\varphi_0 \\ -\sin\theta_0 \sin\varphi_0 \\ -\cos\theta_0 \end{vmatrix}$$

and

$$\boldsymbol{A}_0^\mathrm{e} = \begin{vmatrix} E_x^0 \\ E_y^0 \\ E_z^0 \end{vmatrix} = A^\mathrm{e} \begin{vmatrix} \cos\psi_0 \cos\theta_0 \cos\varphi_0 - \sin\psi_0 \sin\varphi_0 \\ \cos\psi_0 \cos\theta_0 \sin\varphi_0 + \sin\psi_0 \cos\varphi_0 \\ -\cos\psi_0 \sin\theta_0 \end{vmatrix},$$

where $\varphi_0 \in [0, 2\pi]$, $\theta_0 \in [0, (\pi/2)]$, $\psi_0 \in [0, \pi]$, $k_0 = \omega/c$, and $k^+ = \|\boldsymbol{k}^+\| = k_0\sqrt{\varepsilon^+}$.

Let us stress here that the whole development of the method is valid for anisotropic material properties. Even if the material considered here are isotropic, we keep the bold tensor notation $\boldsymbol{\varepsilon}$; and $\boldsymbol{\mu}$; because PMLs can be considered as media with anisotropic and lossy equivalent material properties. We can define the material parameters distribution for the MIM metamaterial denoted $\boldsymbol{\varepsilon} = \varepsilon\boldsymbol{I}$; and $\boldsymbol{\mu} = \mu\boldsymbol{I}$; ($\boldsymbol{I}$; is the identity tensor) as

$$\eta(x,y,z) := \begin{cases} \eta^+ & \text{for} \quad z > 0 \\ \eta_\mathrm{g}(x,y,z) & \text{for} \quad z_1 < z < 0 \\ \eta_\mathrm{Si} & \text{for} \quad z_2 < z < z_1 \\ \eta_\mathrm{Cr} & \text{for} \quad z_3 < z < z_2 \\ \eta^- & \text{for} \quad z < z_3 \end{cases}$$

for $\eta = \{\varepsilon, \mu\}$, with $z_1 = -h_\mathrm{r}$, $z_2 = z_1 - h_\mathrm{i}$ and $z_3 = z_2 - h_\mathrm{m}$.

The so-called diffraction problem we are dealing with is to find nontrivial solutions of Maxwell's equation, i.e., to find the unique electromagnetic field $(\boldsymbol{E}, \boldsymbol{H})$ such that

$$\mathcal{L}_{\boldsymbol{\varepsilon},\boldsymbol{\mu}}(\boldsymbol{E}) := -\nabla \times (\boldsymbol{\mu}^{-1}\nabla \times \boldsymbol{E}) + k_0^2\boldsymbol{\varepsilon}\boldsymbol{E} = \boldsymbol{0}, \tag{1}$$

where the diffracted field $\boldsymbol{E}^d = \boldsymbol{E} - \boldsymbol{E}_0$ satisfies an outgoing wave condition (OWC) and where $\boldsymbol{E}_0$ is the restriction of $\boldsymbol{E}^\mathrm{inc}$ to the superstrate ($\boldsymbol{E}_0 = \boldsymbol{E}^\mathrm{inc}$ for $z > 0$ and $\boldsymbol{E}_0 = \boldsymbol{0}$ elsewhere). The total electric field $\boldsymbol{E}$; is quasiperiodic along x and y:

$$\boldsymbol{E}(x + d_x, y + d_y, z) = \boldsymbol{E}(x,y,z)\mathrm{e}^{i(\alpha d_x + \beta d_y)}.$$

Under this form, the problem is not adapted to a resolution by a numerical method because of infinite issues: The sources of the plane wave are infinitely far above the structure, the geometric domain is unbounded, and the scattering structure is periodic and therefore infinite. To circumvent these issues [33], we compute only the diffracted field solution of an equivalent radiation problem with sources inside the scatterers (the nanorods in our case), we use PMLs to truncate the unbounded domain at a finite distance, and we use quasiperiodicity conditions to model a single period of the grating.

We denote $\boldsymbol{\varepsilon}_1$ and $\boldsymbol{\mu}_1$, the tensor fields describing the multilayer problem [i.e., the same problem as Eq. (1) but without the nanorods]:

$$\eta_1(x,y,z) := \begin{cases} \eta^+ & \text{for} \quad z > z_1 \\ \eta_\mathrm{Si} & \text{for} \quad z_2 < z < z_1 \\ \eta_\mathrm{Cr} & \text{for} \quad z_3 < z < z_2 \\ \eta^- & \text{for} \quad z < z_3 \end{cases},$$

where $\boldsymbol{\eta}_1 = \eta_1\boldsymbol{I}$; for $\eta = \{\varepsilon, \mu\}$. The function $\boldsymbol{E}_1$ is defined as the unique solution of $\mathcal{L}_{\boldsymbol{\varepsilon}_1,\boldsymbol{\mu}_1}(\boldsymbol{E}_1) = 0$, such that $\boldsymbol{E}_1^d := \boldsymbol{E}_1 - \boldsymbol{E}_0$ satisfies an OWC. The expression of this function can be calculated with a matrix transfer formalism extensively used in thin film optics (see for example [34]). The unknown function $\boldsymbol{E}_2^d$ is thus given by $\boldsymbol{E}_2^d = \boldsymbol{E} - \boldsymbol{E}_1 = \boldsymbol{E}^d - \boldsymbol{E}_1^d$. The scattering problem (1) can be rewritten as

$$\mathcal{L}_{\boldsymbol{\varepsilon},\boldsymbol{\mu}}(\boldsymbol{E}_2^d) = -\mathcal{L}_{\boldsymbol{\varepsilon},\boldsymbol{\mu}}(\boldsymbol{E}_1). \tag{2}$$

The term on the right hand side can be seen as a source term $\boldsymbol{\mathcal{S}}_1 := -\mathcal{L}_{\boldsymbol{\varepsilon},\boldsymbol{\mu}}(\boldsymbol{E}_1) = -\mathcal{L}_{\boldsymbol{\varepsilon}-\boldsymbol{\varepsilon}_1,\boldsymbol{\mu}-\boldsymbol{\mu}_1}(\boldsymbol{E}_1)$ because of the linearity of the operator $\mathcal{L}$ and since $\mathcal{L}_{\boldsymbol{\varepsilon}_1,\boldsymbol{\mu}_1}(\boldsymbol{E}_1) = 0$. This source term has support in the nanorods $\Omega_{g'}$ (since the material

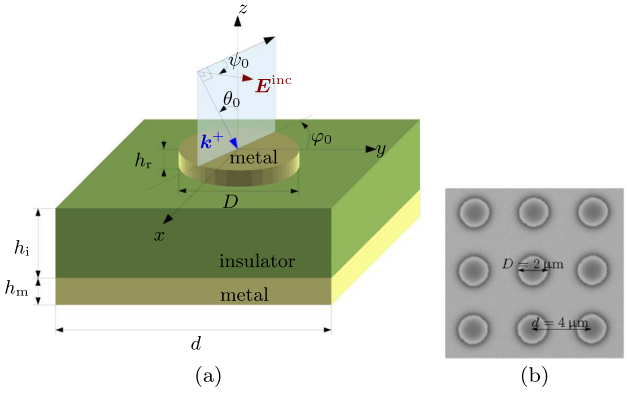

Fig. 1. Geometry of the studied structures. (a) Schematic representation and notations. (b) SEM image (top view) of a fabricated grating.

parameters η and η_1 are equal everywhere else) and is known in closed form [33]. In the case treated here, where the contrast of permeability is null ($\mu = \mu_1 = 1$ everywhere), we have

$$\boldsymbol{\mathcal{S}}_1(\omega, \theta_0, \varphi_0, \psi_0) = k_0^2[\varepsilon^+ - \varepsilon_{\mathrm{Cr}}(\omega)]\boldsymbol{E}_1(\omega, \theta_0, \varphi_0, \psi_0). \quad (3)$$

This source term depends on the incidence parameters and on the permittivity contrast between the superstrate and the nanorod.

The radiation problem defined by Eq. (2) is then solved by the FEM [33,35], using PMLs to truncate the infinite regions and by setting convenient boundary conditions on the outermost limits of the domain. We apply Bloch quasiperiodicity conditions with coefficient α (resp. β) on the two parallel boundaries orthogonal to x (resp. y) and homogeneous Dirichlet boundary conditions on the outward boundary of the PMLs. The computational cell is meshed using second-order edge elements. The final algebraic system is solved using a direct solver (PARDISO [36]).

B. Spectral Problem

The diffractive properties of open waveguides such as those studied here are governed by their eigenmodes and eigenfrequencies. The eigenproblem we are dealing with consists in finding the solutions of source free Maxwell's equations, i.e., finding eigenvalues $\Lambda_n = (\omega_n/c)^2$ and nonzero eigenvectors $\boldsymbol{V}_n$ such that

$$\mathcal{M}_{\boldsymbol{\mu}}(\boldsymbol{V}_n) := \nabla \times (\boldsymbol{\mu}^{-1}\nabla \times \boldsymbol{V}_n) = \Lambda_n \boldsymbol{\varepsilon} \boldsymbol{V}_n. \quad (4)$$

Note that we search for Bloch–Floquet eigenmodes so Maxwell's operator $\mathcal{M}_{\boldsymbol{\mu}}$ is parametrized by the real quasiperiodicity coefficients α and β. Because we are dealing with an open structure, the eigenvalues Λ_n are complex even for Hermitian materials. The spectrum of the associated Maxwell's operator is constituted of a continuous part (which is composed of a denombrable set of branches for periodic structures and that is real for lossless semi infinite substrate and superstrate) corresponding to radiation modes and a discrete set of complex eigenvalues associated with the so-called quasimodes (also known as leaky modes or resonant states). PMLs have proven to be a very convenient tool to compute leaky modes in various configurations [37–40] because they mimic efficiently the infinite space provided an appropriate choice of their parameters. The complex coordinate stretch used for (theoretically infinite) PML provide the suitable non-Hermitian extention of Maxwell's operator to compute quasimodes. As detailed in [28], if we choose a constant stretching parameter ζ for the PMLs, it is sufficient to take $\Re\mathrm{e}(\zeta) > 0$ and $\Im\mathrm{m}(\zeta) > 0$ to rotate by an angle proportional to $\gamma = -\arg\zeta$ the continuous spectrum in the lower half complex plane $\Re\mathrm{e}(\omega) < 0$, which "reveals" *outgoing* quasimodes (satisfying outgoing wave conditions). It is well known that the associated eigenvalues are *poles* of the scattering matrix. In addition, the *zeros* Λ_n^z of the scattering matrix are associated with *incoming* quasimodes [21] (satisfying incoming wave conditions) that we can compute by setting $\Re\mathrm{e}(\zeta) > 0$ and $\Im\mathrm{m}(\zeta) < 0$, leading to a rotation of the continuous spectrum in the upper half complex plane $\Re\mathrm{e}(\omega) > 0$ [28]. A real zero Λ^z indicates total absorption of incident light. Finally, PMLs are truncated at a finite distance where the electromagnetic field has decreased to a negligible value because the computational domain needs to be of finite extent to apply the FEM, which results in a discretization of the continuous spectrum [41]. Note that the incident angles θ_0 et φ_0 appear in a subtle way through the quasiperiodicity coefficients α et β, but the polarization angle ψ_0 *does not come into play in the spectral problem*. It is thus necessary to thoroughly study eigenmodes in order to find the polarization state that can excite the modes at stake.

The eigenvalue problem defined by Eq. (4) is solved with the FEM, as described in Section 2.A. We have supposed here that the materials are nondispersive, which makes the problem in Eq. (4) linear. To take into account dispersion, the eigenvalue problem is solved iteratively with updated values of permittivity. This procedure converges rapidly due to the slow variations of the permittivity of the considered materials in the far infrared range.

C. Quasimodal Expansion Method

We first define the classical inner product of two functions $\boldsymbol{F}$; and $\boldsymbol{G}$; of $L^2(\Omega)$, $\Omega \subset \mathbb{R}^3$:

$$\langle \boldsymbol{F} | \boldsymbol{G} \rangle := \int_\Omega \boldsymbol{F}(\boldsymbol{r}) \cdot \overline{\boldsymbol{G}(\boldsymbol{r})} \mathrm{d}\boldsymbol{r}. \quad (5)$$

Because it is non-self-adjoint, we have $\langle \boldsymbol{\varepsilon} \boldsymbol{V}_n | \boldsymbol{V}_m \rangle \neq \delta_{nm}$; in other words the eigenmodes $\boldsymbol{V}_n$ are not orthogonal with respect to this standard definition. This is the reason why we consider an adjoint spectral problem with eigenvalues $\overline{\Lambda_n} = (\overline{\omega_n}/c)^2$ and eigenvectors $\boldsymbol{W}_n$. The adjoint operator $\mathcal{M}_{\boldsymbol{\mu}}^\dagger$ is defined by

$$\langle \mathcal{M}_{\boldsymbol{\mu}}(\boldsymbol{V}) | \boldsymbol{W} \rangle = \langle \boldsymbol{V} | \mathcal{M}_{\boldsymbol{\mu}}^\dagger(\boldsymbol{W}) \rangle, \quad (6)$$

with *complex conjugate coefficients* for the boundary conditions in comparison with the direct spectral problem [42] and is such that $\mathcal{M}_{\boldsymbol{\mu}}^\dagger = \mathcal{M}_{\boldsymbol{\mu}^\star}$, where $A^\star = \bar{A}^{\mathrm{T}}$ is the conjugate transpose of matrix A. The associated adjoint problem that we shall solve is

$$\mathcal{M}_{\boldsymbol{\mu}}^\dagger(\boldsymbol{W}_n) = \nabla \times (\boldsymbol{\mu}^{\star -1}\nabla \times \boldsymbol{W}_n) = \overline{\Lambda_n} \boldsymbol{\varepsilon}^\star \boldsymbol{W}_n. \quad (7)$$

We know from spectral theory that the eigenvectors $\boldsymbol{V}_n$ are bi-orthogonal to their adjoint counterparts $\boldsymbol{W}_n$ [43]:

$$\langle \boldsymbol{\varepsilon} \boldsymbol{V}_n | \boldsymbol{W}_m \rangle := \int_\Omega \boldsymbol{\varepsilon}(\boldsymbol{r}) \boldsymbol{V}_n(\boldsymbol{r}) \cdot \overline{\boldsymbol{W}_m(\boldsymbol{r})} \mathrm{d}\boldsymbol{r} = K_n \delta_{nm}, \quad (8)$$

where the normalization coefficient $K_n = \boldsymbol{\varepsilon}\langle \boldsymbol{V}_n | \boldsymbol{W}_n \rangle$. Relation (8) provides a bi-orthogonal set to expand every field solution of Eq. (2) propagating in the open waveguide as

$$\boldsymbol{E}_2^d(\boldsymbol{r}, \omega, \psi) = \sum_{n=1}^{+\infty} P_n(\omega, \psi) \boldsymbol{V}_n(\boldsymbol{r}) + \int_{\Gamma_c} P_\nu(\omega, \psi) \boldsymbol{V}_\nu(\boldsymbol{r}) \mathrm{d}\nu, \quad (9)$$

where Γ_c is the continuous spectrum (a curve, with possibly a denombrable set of branches in the complex plane). The coefficients $P_k(\omega, \psi)$, $k = \{n, \nu\}$, are given by

$$P_k(\omega, \psi) = \frac{1}{K_k} \langle \boldsymbol{\varepsilon} \boldsymbol{E}_2^d | \boldsymbol{W}_k \rangle = \frac{J_k(\omega, \psi)}{\omega^2 - \omega_k^2}, \quad (10)$$

with

$$J_k(\omega,\psi) = \frac{c^2}{K_k}\langle \boldsymbol{\mathcal{S}}_1 | \boldsymbol{W}_k \rangle = \frac{c^2}{K_k}\int_{\Omega_{g'}} \boldsymbol{\mathcal{S}}_1(\boldsymbol{r},\omega,\psi)\overline{\boldsymbol{W}_k(\boldsymbol{r})}\mathrm{d}\boldsymbol{r}, \quad (11)$$

where the integration is *only performed on the nanorod* $\Omega_{g'}$ since the source term $\boldsymbol{\mathcal{S}}_1$ is zero elsewhere.

We are thus able to know how a given mode is excited when changing the incident field. This modal expansion can be approximated by a discrete sum since the spectrum of the final operator we solve for involves only discrete eigenfrequencies, and in practice only a finite number M of modes is retained in the expansion, so that we can write

$$\boldsymbol{E}_2^d(\boldsymbol{r},\omega,\psi) \simeq \sum_{m=1}^{M} P_m(\omega,\psi)\boldsymbol{V}_m(\boldsymbol{r}). \quad (12)$$

This leads to a reduced modal representation of the field that is well adapted when studying the resonant properties of the open structure, as illustrated in the sequel.

3. NUMERICAL AND EXPERIMENTAL STUDY OF MIM ARRAYS

The parameters employed are $h_r = 100$ nm, $h_i = 530$ nm, $h_m = 200$ nm, and we fix the ratio between the rod diameter and the period $f = D/d = 0.5$. We study the influence of the period d on the reflection spectrum of the metamaterial.

A. Fabrication and Characterization of the Samples

Samples with parameters described above and varying period of 4.0, 4.4, 4.8, 5.2, and 5.6 μm have been fabricated [a SEM image showing a top view of the filter with $d = 4$ μm is given in Fig. 1(b)]. The different layers have been deposited by magnetron sputtering on a standard silicon wafer of diameter 100 mm and thickness 525 μm. Large area samples (1 cm × 1 cm) were patterned with a standard photolithography process with a positive resist deposition followed by a chemical etching of the top chromium layer.

Reflection spectra have been recorded with a Thermo Fisher-Nicolet 6700 Fourier transform infrared (FTIR) spectrophotometer. The measurements were performed with a focused unpolarized light beam with ±16° divergence and a spot diameter of 4 mm. An accessory composed of a set of mirrors allows us to record reflection spectrum for incident angles between 0° and 90°. All the spectra are normalized with a background recorded from a reference gold mirror.

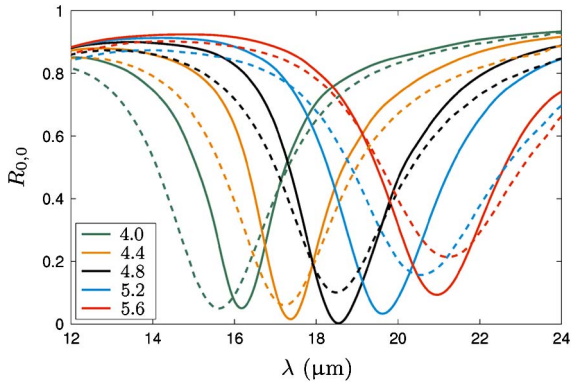

Fig. 2. Reflection spectrum at normal incidence in the specular order $R_{0,0}$ as a function of incident wavelength λ for different values of the period d (in μm). Solid lines, full wave FEM simulations; dashed lines, FTIR measurements.

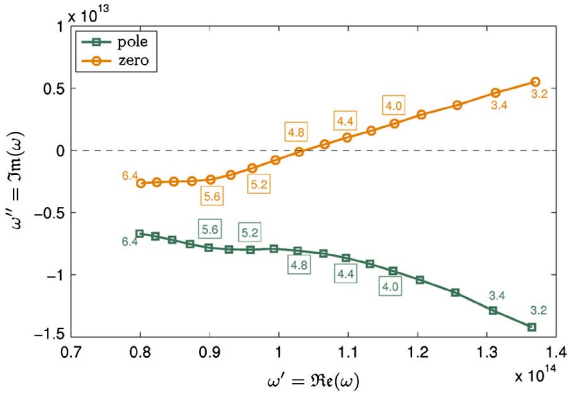

Fig. 3. Location of pole (green squares) and zero (orange circles) in the complex plane as a function of d (we only represented the pole and zero of the TE mode because of degeneracy). The values of d are indicated in μm, and the boxed values indicates the fabricated structures. The black dashed line represents the real axis.

B. Reflection Spectra

Figure 2 shows the reflection spectra at normal incidence in the specular order for bi-gratings with different periods, calculated by the FEM formulation described in Section 2.A

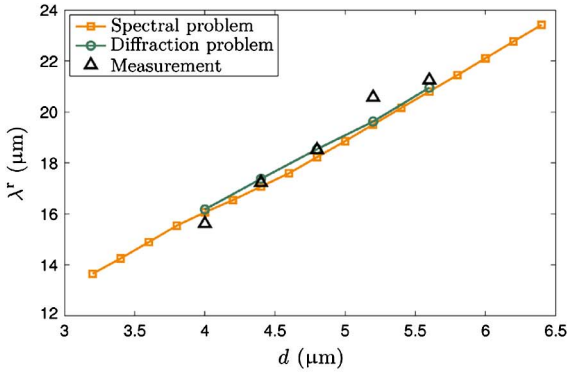

(a) Resonant wavelength.

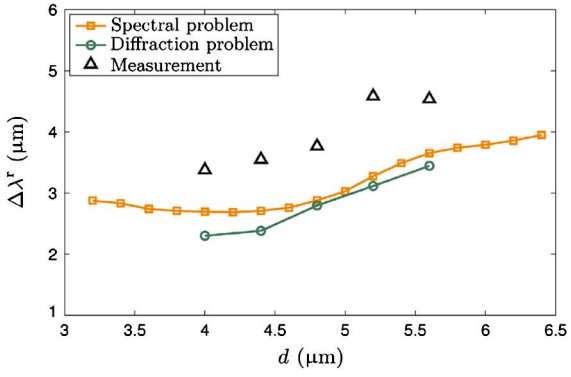

(b) Spectral width.

Fig. 4. Spectral parameters of the resonance as a function of the period d obtained with different methods: extracted from calculated (green circles) and measured (black triangles) reflection spectra and extracted from the pole eigenfrequency (orange squares). (a) Resonant wavelength and (b) spectral width.

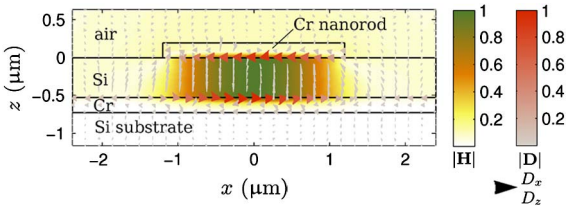

Fig. 5. Field map of the TE outgoing leaky mode in the Oxz plane for $d = 4.8$ μm. The left colormap represents the norm of the magnetic field $\boldsymbol{H}$;, the arrows represent the direction of the displacement current $\boldsymbol{D}$; and their colors (right colormap) and size are proportional to its intensity.

(solid lines). These spectra show a clear resonant behavior in the region 12–24 μm with a large reflection dip. Increasing the period d shifts this dip to larger wavelengths and broadens the resonance. It can also be noted that for $d = 4.8$ μm, the reflection is almost zero at resonance. Since the transmission is negligible because the thickness of the bottom metal layer is nearly twice the skin depth of chromium in this spectral range, the incident power is nearly totally absorbed by the metamaterial at resonance and dissipated by Joule heating.

The measured reflection spectra of the fabricated samples are reported in Fig. 2 (dashed curves) and show good agreement with numerical simulations. For example for $d = 4.8$ μm, both experimental and simulated reflection dips are located at 18.5 μm, although experimentally, the reflection minimum is 10%, more than the 0.3% simulated value. For all samples, the disagreements originates from spectral broadening of the measured reflection. We have checked numerically that the spectral position of the resonance is largely affected by slights variations on the rod diameter. The study of SEM images over our samples showed that the rods were uniformly spaced (good tolerance on the periodicity) but that there were size dispersion on the rod diameter over the fabricated samples, leading to different resonances position for each

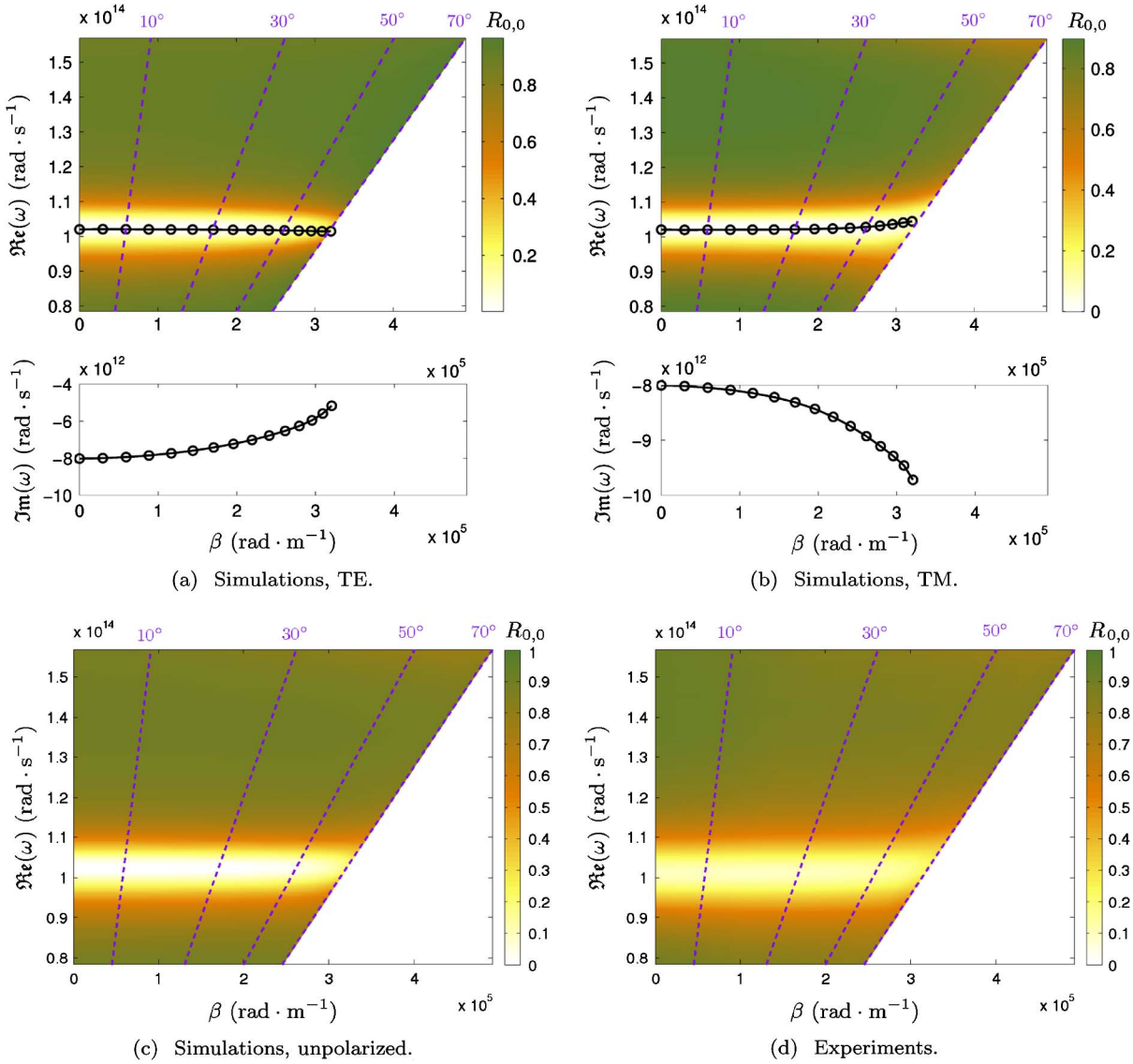

Fig. 6. Influence of the incidence. Colormap: reflection spectrum in the specular order $R_{0,0}$ as a function of frequency ω and quasiperiodicity coefficient β for $d = 4.8$ μm. (a) Simulations, TE polarization; (b) simulations, TM polarization; (c) simulations, unpolarized; and (d) FTIR measurements. In (a) and (b), the black circles indicate the real (top) and imaginary (bottom) parts of the eigenfrequency ω_1 of the corresponding leaky mode as a function of β.

resonator and finally to a spectral broadening of the reflection dip.

C. Influence of the Periodicity: A Pole-Zero Approach

To highlight the resonant properties of the studied MIM arrays, we report here a modal analysis of such structures. We solved numerically the spectral problem (4) as described in Section 2.B, with quasiperiodicity coefficients $\alpha = \beta = 0$. Because of the symmetry of the problem in these conditions, we find two degenerate outgoing leaky modes (associated with poles of the complex reflection coefficient $r_{0,0}$) and two degenerate incoming leaky modes (associated with zeros of $r_{0,0}$). The degenerescence corresponds to eigenmodes with TE and TM polarization.

Figure 3 shows the evolution of the pole and its associated zero in the complex ω-plane as a function of d (we only represented the pole and zero of the TE mode because of degeneracy). The real parts of the pole and of the zero are almost equal and shift to smaller frequencies as the period increases. For $d = 4.8$ μm, the zero crosses the real axis, which means that the reflection is suppressed for a real incident frequency close to this zero. This is consistent with the previous observations from reflection spectra.

We reported in Fig. 4 the values of the resonant wavelength and the spectral width of the resonances extracted from the calculated (green circles) and from measured (black triangles) reflection spectra, as well as those derived from the pole eigenfrequencies (orange squares). As it can be seen in Fig. 4(a), the position of the resonance increases linearly with d, with the values calculated from simulated reflection spectra minima and from the spectral problem being in excellent agreement, which indicates that the resonant reflection dip stems from the excitation of the leaky mode associated with this eigenfrequency. In addition, experimental values well agree with the positions predicted by the two numerical approaches. Moreover, the spectral width of the dip increases with d, as can be seen in Fig. 4(b). In that case, the values obtained from the diffraction problem and from the spectral problem are in good agreement but slightly differs because the spectral width extracted from reflection spectra may be influenced by the presence of other modes, whereas the linewidth associated with a leaky mode is valid for an isolated resonance. The experimental values are larger, as said before, but show a variation with d similar to the calculated ones.

To highlight the physical mechanism responsible for these resonant total absorption (or equivalently suppressed reflection), we plotted in Fig. 5 the magnetic field associated with the TE outgoing quasimode for $d = 4.8$ μm. The electric displacement represented by arrows is very strong with opposite directions in the rod and the metal layer, which creates a strong magnetic response (see colormap) confined in the silicon layer below the nanorod. Note that the nature of the resonance is not related to Fabry–Perot type mechanism because the silicon layer is very thin ($<\lambda/30$), but rather to localized electric and magnetic dipoles [8].

D. Angular Tolerance

One of the key features of MIM arrays is the angular tolerance of the first order resonance, which is crucial for filtering applications. The colormap in Fig. 6 shows the reflection spectrum as function of frequency ω and transverse wavenumber β for $d = 4.8$ μm. Figures 6(a) and 6(b) are calculated values in TE and TM polarization, respectively. We also plotted the evolution of the real part ω_1' of the eigenfrequency ω_1 associated with either TE or TM mode, the so-called dispersion diagram. In both cases, the real part of the eigenfrequency remains almost constant, with a slight redshift (resp. blueshift) for TM (resp. TE) polarization at large angles and matches well the position of the resonant reflection dip. As β increases, the

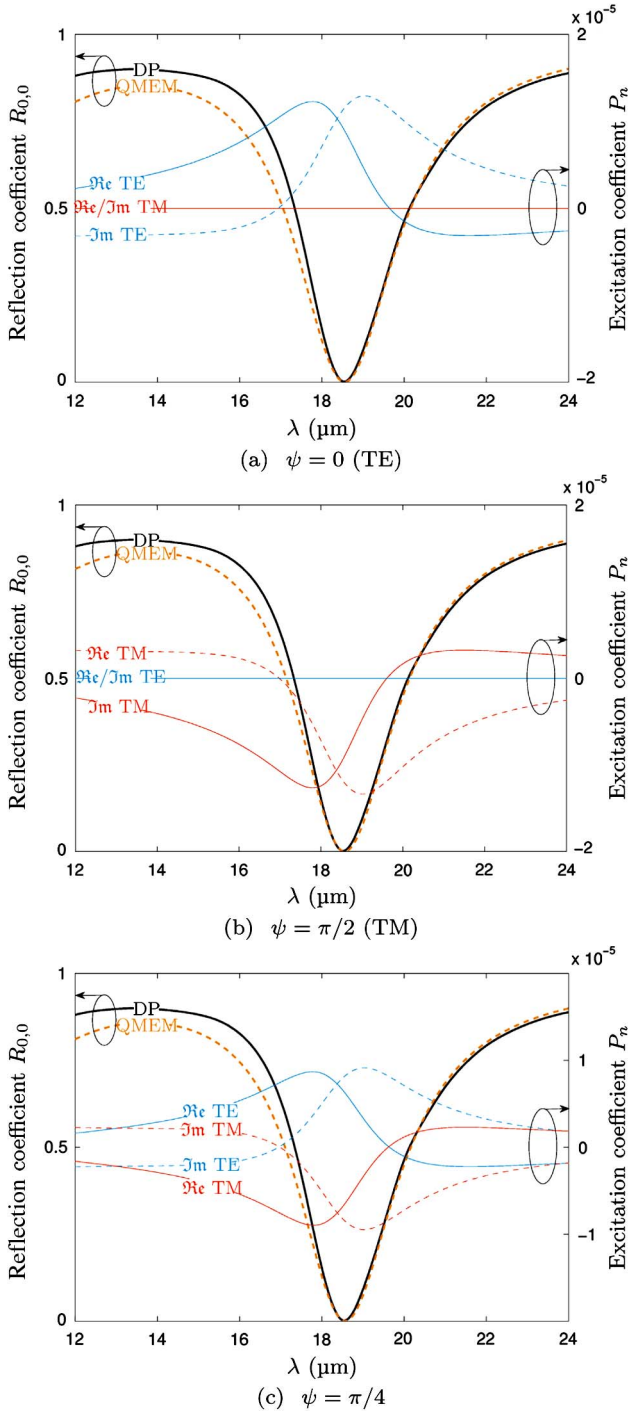

Fig. 7. Excitation coefficients P_n for the two degenerate modes (right ordinate, TE blue, TM red, real parts: solid line, imaginary part: dashed line) and reflection coefficient $R_{0,0}$ computed with full wave FEM diffraction problem (DP, black solid line) and with the QMEM with these two modes (orange dashed line).

resonance sharpens in the TE case and broadens in the TM case. These observations are confirmed by the evolution of imaginary part ω_1'' of eigenfrequencies [see bottom plot in Figs. 6(a) and 6(b)], because the real part ω' is almost constant the quality factor of the resonance $Q = \omega'/\Delta\omega = \omega_1'/2\omega_1''$ increases (resp. decreases) for TE (resp. TM) polarization. To compare with experimental results of Fig. 6(d), we also plotted the calculated unpolarized case in Fig. 6(c). The agreement between simulations and measurements is excellent except a slight spectral broadening and higher minimum values for experimental results and demonstrates the angular tolerance up to 70° of the fabricated filters.

E. Leaky Mode Excitation and Minimal Resonant Model

Finally, we computed the diffracted field using Eq. (12) with the two leaky modes TE and TM. Because of the mode degeneracy, every linear combination of the two eigenmodes is also the solution of Eq. (4) for the eigenvalue denoted $\omega_1 = \omega_1' + i\omega_1''$. We define the TE mode such that $J_{\mathrm{TE}}(\omega_1', \psi_{\mathrm{TE}}) = 1$ and $J_{\mathrm{TE}}(\omega_1', \psi_{\mathrm{TM}}) = 0$, where $\psi_{\mathrm{TE}} = 0$ and $\psi_{\mathrm{TM}} = \pi/2$. The TM mode is then obtained by standard Gram–Schmidt orthogonalization procedure, and the two modes are finally normalized such that $K_{\mathrm{TE}} = K_{\mathrm{TM}} = 1$.

The study of the coupling coefficients P_n reveals the resonant nature of the interaction of a plane wave with the modes. In Fig. 7, we plot these coefficients as a function of wavelength for different polarization cases: (a) $\psi = 0$ (TE), (b) $\psi = \pi/2$ (TM), and (c) $\psi = \pi/4$. The real (solid line) and imaginary (dashed line) parts of the excitation coefficients show strong variations around the resonant frequency in all cases. For $\psi = 0$ (resp. $\psi = \pi/2$), only the TE (resp. TM) mode is excited while the value of P_n for the TM (resp. TE) mode is negligible. For $\psi = \pi/4$, both modes participate equally to the resonant diffraction process as their coupling coefficients are equal in absolute value (opposite sign is arbitrarily set for display purpose). These observations illustrate the independence of the reflection dip with regards to polarization. We have also computed $R_{0,0}$ with the field reconstructed by the quasimodal expansion method (QMEM) with only two leaky modes. The results (orange dashed line in Fig. 7) are in all cases in excellent agreement with full wave FEM simulations of the diffraction problem (DP, black solid line). This means that the diffractive properties of the structure are dominated by these two modes in the considered wavelength range. The small discrepancies at small wavelengths are attributed to other modes with higher resonant frequencies not taken into account in the minimal resonant model.

4. CONCLUSION

We have studied metamaterial based on MIM designed to serve as reflection bandcut filters in the thermal infrared spectral range. These structures show quasi-total absorption of light at the resonant wavelength that can be tuned by varying the lateral dimensions of the metallic nanorods grating. The reflection dip spectral position is also independent of incident angle up to 70° and is not affected by the polarization state of the incident light. Our study provides an in-depth modal analysis revealing the resonant nature of the interaction of light with leaky modes of the structure. We developed a QMEM that allows us to compute coupling coefficients between a plane wave and the modes. This method leads to a minimal resonant model with two modes that fits well full wave FEM diffraction problem simulations. Large area samples have been fabricated and FTIR measured reflection spectra are in good agreement with the different numerical approaches, demonstrating the potential practical application of those polarization independent and angular tolerant resonant filters. Although the filters studied here have been designed to work between 15 and 22 μm, the concepts studied here can be applied to higher frequency ranges (e.g., band III of the infrared between 7 and 13 μm) by scaling down the dimensions of the structures.

ACKNOWLEDGMENTS

This research was financially supported by the Fonds Unique Interministériel (FUI) and by a CIFRE fellowship from the French Agence Nationale de la Recherche et de la Technologie (ANRT). Part of the components were realized within the framework of the Espace Photonique facility at Institut Fresnel with the financial support of the French Department of Industry, the local administration (Provence-Alpes Côte d'Azur Regional Council), CNRS, and the European Community.

REFERENCES AND NOTES

1. R. W. Wood, "On a remarkable case of uneven distribution of light in a diffraction grating spectrum," Proc. Phys. Soc. London **18**, 269–275 (1902).
2. M. Hutley and D. Maystre, "The total absorption of light by a diffraction grating," Opt. Commun. **19**, 431–436 (1976).
3. A. Hessel and A. A. Oliner, "A new theory of Wood's anomalies on optical gratings," Appl. Opt. **4**, 1275–1297 (1965).
4. T. V. Teperik, F. J. Garcia de Abajo, A. G. Borisov, M. Abdelsalam, P. N. Bartlett, Y. Sugawara, and J. J. Baumberg, "Omnidirectional absorption in nanostructured metal surfaces," Nat. Photonics **2**, 299–301 (2008).
5. N. I. Landy, S. Sajuyigbe, J. J. Mock, D. R. Smith, and W. J. Padilla, "Perfect metamaterial absorber," Phys. Rev. Lett. **100**, 207402 (2008).
6. N. Bonod, G. Tayeb, D. Maystre, S. Enoch, and E. Popov, "Total absorption of light by lamellar metallic gratings," Opt. Express **16**, 15431–15438 (2008).
7. H. Tao, N. I. Landy, C. M. Bingham, X. Zhang, R. D. Averitt, and W. J. Padilla, "A metamaterial absorber for the terahertz regime: design, fabrication and characterization," Opt. Express **16**, 7181–7188 (2008).
8. J. Hao, J. Wang, X. Liu, W. J. Padilla, L. Zhou, and M. Qiu, "High performance optical absorber based on a plasmonic metamaterial," Appl. Phys. Lett. **96**, 251104 (2010).
9. N. Liu, M. Mesch, T. Weiss, M. Hentschel, and H. Giessen, "Infrared perfect absorber and its application as plasmonic sensor," Nano Lett. **10**, 2342–2348 (2010).
10. T. Maier and H. Brückl, "Wavelength-tunable microbolometers with metamaterial absorbers," Opt. Lett. **34**, 3012–3014 (2009).
11. T. Maier and H. Brueckl, "Multispectral microbolometers for the midinfrared," Opt. Lett. **35**, 3766–3768 (2010).
12. K. Aydin, V. E. Ferry, R. M. Briggs, and H. A. Atwater, "Broadband polarization-independent resonant light absorption using ultrathin plasmonic super absorbers," Nat. Commun. **2**, 517 (2011).
13. J. Hao, L. Zhou, and M. Qiu, "Nearly total absorption of light and heat generation by plasmonic metamaterials," Phys. Rev. B **83**, 165107 (2011).
14. P. Bouchon, C. Koechlin, F. Pardo, R. Haïdar, and J.-L. Pelouard, "Wideband omnidirectional infrared absorber with a patchwork of plasmonic nanoantennas," Opt. Lett. **37**, 1038–1040 (2012).
15. J. Yang, C. Sauvan, A. Jouanin, S. Collin, J.-L. Pelouard, and P. Lalanne, "Ultrasmall metal-insulator-metal nanoresonators: impact of slow-wave effects on the quality factor," Opt. Express **20**, 16880–16891 (2012).

16. E. Popov, L. Mashev, and D. Maystre, "Theoretical study of the anomalies of coated dielectric gratings," J. Mod. Opt. **33**, 607–619 (1986).
17. M. Nevière, E. Popov, and R. Reinisch, "Electromagnetic resonances in linear and nonlinear optics: phenomenological study of grating behavior through the poles and zeros of the scattering operator," J. Opt. Soc. Am. A **12**, 513–523 (1995).
18. S. G. Tikhodeev, A. L. Yablonskii, E. A. Muljarov, N. A. Gippius, and T. Ishihara, "Quasiguided modes and optical properties of photonic crystal slabs," Phys. Rev. B **66**, 045102 (2002).
19. A.-L. Fehrembach and A. Sentenac, "Study of waveguide gratings eigenmodes for unpolarized filtering applications," J. Opt. Soc. Am. A **20**, 481–488 (2003).
20. P. Lalanne, J. P. Hugonin, and P. Chavel, "Optical properties of deep lamellar gratings: a coupled Bloch-mode insight," J. Lightwave Technol. **24**, 2442 (2006).
21. V. Grigoriev, S. Varault, G. Boudarham, B. Stout, J. Wenger, and N. Bonod, "Singular analysis of Fano resonances in plasmonic nanostructures," Phys. Rev. A **88**, 063805 (2013).
22. A. L. Fehrembach and A. Sentenac, "Unpolarized narrow-band filtering with resonant gratings," Appl. Phys. Lett. **86**, 121105 (2005).
23. A. Sentenac and A.-L. Fehrembach, "Angular tolerant resonant grating filters under oblique incidence," J. Opt. Soc. Am. A **22**, 475–480 (2005).
24. Y. Ding and R. Magnusson, "Resonant leaky-mode spectral-band engineering and device applications," Opt. Express **12**, 5661–5674 (2004).
25. Y. Ding and R. Magnusson, "Doubly resonant single-layer bandpass optical filters," Opt. Lett. **29**, 1135–1137 (2004).
26. Y. Ding and R. Magnusson, "Use of nondegenerate resonant leaky modes to fashion diverse optical spectra," Opt. Express **12**, 1885–1891 (2004).
27. M. B. Doost, W. Langbein, and E. A. Muljarov, "Resonant state expansion applied to two-dimensional open optical systems," Phys. Rev. A **87**, 043827 (2013).
28. B. Vial, F. Zolla, A. Nicolet, and M. Commandré, "Quasimodal expansion of electromagnetic fields in open two-dimensional structures," Phys. Rev. A **89**, 023829 (2014).
29. C. Sauvan, J. P. Hugonin, I. S. Maksymov, and P. Lalanne, "Theory of the spontaneous optical emission of nanosize photonic and plasmon resonators," Phys. Rev. Lett. **110**, 237401 (2013).
30. Q. Bai, M. Perrin, C. Sauvan, J.-P. Hugonin, and P. Lalanne, "Efficient and intuitive method for the analysis of light scattering by a resonant nanostructure," Opt. Express **21**, 27371–27382 (2013).
31. R. Lovrinčić and A. Pucci, "Infrared optical properties of chromium nanoscale films with a phase transition," Phys. Rev. B **80**, 205404 (2009).
32. E. D. Palik, *Handbook of Optical Constants of Solids* (Academic, 1991).
33. G. Demésy, F. Zolla, A. Nicolet, and M. Commandré, "All-purpose finite element formulation for arbitrarily shaped crossed-gratings embedded in a multilayered stack," J. Opt. Soc. Am. A **27**, 878–889 (2010).
34. H. MacLeod, *Thin-Film Optical Filters*, 3rd ed. (Institute of Physics, 2001).
35. G. Demésy, F. Zolla, A. Nicolet, and M. Commandré, "Versatile full-vectorial finite element model for crossed gratings," Opt. Lett. **34**, 2216–2218 (2009).
36. O. Schenk and K. Gärtner, "Solving unsymmetric sparse systems of linear equations with PARDISO," Future Gener. Comput. Syst. **20**, 475–487 (2004).
37. Y. Ould Agha, F. Zolla, A. Nicolet, and S. Guenneau, "On the use of PML for the computation of leaky modes: an application to gradient index MOF," COMPEL **27**, 95–109 (2008).
38. M. Popovic, "Complex-frequency leaky mode computations using PML boundary layers for dielectric resonant structures," in *Integrated Photonics Research*, OSA Technical Digest (Optical Society of America, 2003), paper ITuD4.
39. S. Hein, T. Hohage, and W. Koch, "On resonances in open systems," J. Fluid Mech. **506**, 255–284 (2004).
40. M. V. Eliseev, A. G. Rozhnev, and A. B. Manenkov, "Guided and leaky modes of complex waveguide structures," J. Lightwave Technol. **23**, 2586 (2005).
41. F. Olyslager, "Discretization of continuous spectra based on perfectly matched layers," SIAM J. Appl. Math. **64**, 1408–1433 (2004).
42. Actually, the boundary conditions employed here are identical for both spectral problems since we use only real valued coefficients (homogeneous Neumann boundary condition and real quasi-periodicity constants α and β).
43. G. Hanson and A. Yakovlev, *Operator Theory for Electromagnetics: An Introduction* (Springer, 2002).